Tuning Molecular Interactions for Highly Reproducible and Efficient Formamidinium Perovskite Solar Cells via Adduct Approach

Jin-Wook Lee,[†,⊥] Zhenghong Dai,[†,⊥] Changsoo Lee,[‡] Hyuck Mo Lee,[‡] Tae-Hee Han,[†]
Nicholas De Marco,[†] Oliver Lin,[†] Christopher S. Choi,[†] Bruce Dunn,[†] Jaekyung Koh,[§] Dino Di Carlo,[§]
Jeong Hoon Ko,[∥] Heather D. Maynard,[∥] and Yang Yang*,[†]

[†]Department of Materials Science and Engineering and California NanoSystems Institute, University of California, Los Angeles, California 90095, United States
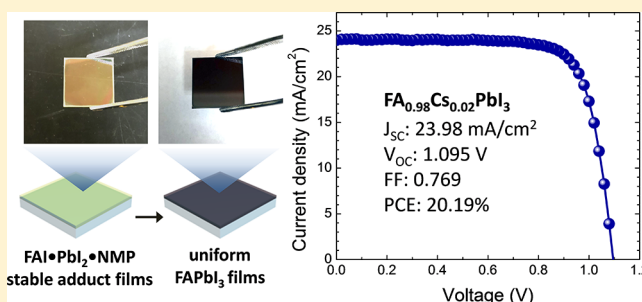
[‡]Department of Materials Science and Engineering, KAIST, 291 Daehak-ro, Yuseong-gu, Daejeon, 305-701, Republic of Korea

[§]Department of Bioengineering and California NanoSystems Institute, University of California, Los Angeles, California 90095, United States

[∥]Department of Chemistry and Biochemistry and California NanoSystems Institute, University of California, Los Angeles, California 90095, United States

S Supporting Information

ABSTRACT: The Lewis acid−base adduct approach has been widely used to form uniform perovskite films, which has provided a methodological base for the development of high-performance perovskite solar cells. However, its incompatibility with formamidinium (FA)-based perovskites has impeded further enhancement of photovoltaic performance and stability. Here, we report an efficient and reproducible method to fabricate highly uniform $FAPbI_3$ films via the adduct approach. Replacement of the typical Lewis base dimethyl sulfoxide (DMSO) with N-methyl-2-pyrrolidone (NMP) enabled the formation of a stable intermediate adduct phase,

which can be converted into a uniform and pinhole-free $FAPbI_3$ film. Infrared and computational analyses revealed a stronger interaction between NMP with the FA cation than DMSO, which facilitates the formation of a stable $FAI \cdot PbI_2 \cdot NMP$ adduct. On the basis of the molecular interactions with different Lewis bases, we proposed criteria for selecting the Lewis bases. Owed to the high film quality, perovskite solar cells with the highest PCE over 20% (stabilized PCE of 19.34%) and average PCE of 18.83 ± 0.73% were demonstrated.

INTRODUCTION

Pioneering efforts to incorporate perovskite (PVSK) materials into a photovoltaic device inspired researchers to develop a solid-state version of PVSK solar cells in 2009.[1−4] The revolutionary elongated lifetime of the solid-state PVSK solar cells facilitated tremendous follow-up research, which has resulted in the rapid evolution of power conversion efficiency (PCE) up to 22.7%.[5] Along with the excellent optoelectronic properties of the PVSK materials, such as high absorption coefficients,[6] long charge carrier lifetime,[7,8] and defect tolerance,[9] low formation enthalpy of the PVSK materials has enabled diverse approaches to fabricate high-quality PVSK thin films and devices.[10]

Organolead halide PVSKs are typically synthesized from the reaction of Pb(II) halides with organic halides. Due to the low formation enthalpy and hygroscopic nature of precursors, the crystallization process should be carefully controlled to obtain uniform and pinhole-free films. Utilization of intermediate phases can facilitate control of nucleation and growth by adjusting activation energy and growth kinetics.[11] Among the coating methods, an adduct approach is widely used to form a

homogeneous PVSK layer.[11−14] Pb(II) halides are known to be Lewis acids, which can form adducts with Lewis bases. For example, a uniform $MAPbI_3$ (MA = CH_3NH_3) PVSK layer can be reproducibly formed using an intermediate $MAI \cdot PbI_2 \cdot DMSO$ adduct.[12] Dimethyl sulfoxide (DMSO) is used as a Lewis base to form the adduct, in which an oxygen bearing lone pair electrons in DMSO forms a coordinative covalent bond with PbI_2 and MAI. A PCE exceeding 20% was demonstrated using the adduct approach.[15] An analogous method has been tried to form a $FAPbI_3$ (FA = $HC(NH_2)_2$) PVSK layer. However, the quality of the $FAPbI_3$ film formed using the adduct approach was relatively poor, which results in a steady-state PCE as low as 14%.[13,16] According to infrared spectroscopy, DMSO was found to be unable to form a stable adduct with FAI, so the resulting $FAPbI_3$ films were relatively less uniform and reproducible compared to $MAPbI_3$ films.[13] Although such a problem has been relieved by tuning the composition of PVSK materials,[17,18] compositional

engineering has accompanied other issues such as phase segregation and increased bandgap.[19,20] Considering the superior optoelectronic properties and stability of the FAPbI$_3$ over MAPbI$_3$,[6,16,21] there is an urgent demand for the development of an effective and reproducible method to form high-quality FAPbI$_3$ films and devices.

In this study, we developed an efficient method to form a highly uniform and reproducible FAPbI$_3$ PVSK film using the adduct approach. A Lewis base *N*-methyl-2-pyrrolidone (NMP) was utilized to form a stable adduct phase with FAI and PbI$_2$. Highly uniform and pinhole-free FAPbI$_3$ PVSK films were fabricated from a FAI·PbI$_2$·NMP intermediate adduct phase. Formation of the adduct was evidenced by infrared spectroscopy, which correlated to density functional theory (DFT) calculation results. Owed to high uniformity and desirable morphology, a PCE over 20% (stabilized PCE of 19.34%) and average PCE of 18.83 ± 0.73% were demonstrated.

■ RESULTS AND DISCUSSION

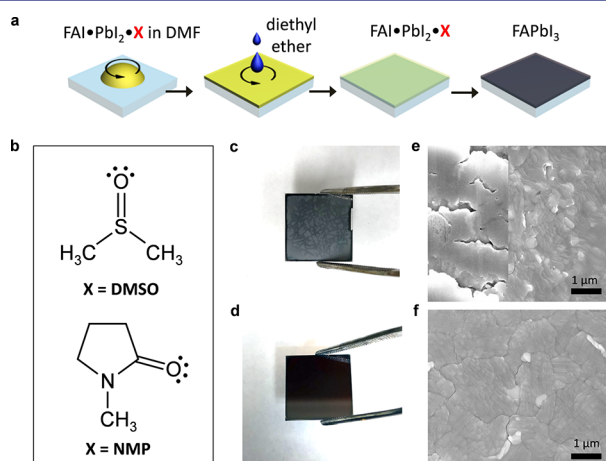**Effect of Lewis Bases on Film Morphology.** A schematic in Figure 1a depicts a typical spin-coating process for the

Figure 1. Effect of Lewis bases on the morphology of FAPbI$_3$ films. (a) A schematic process for formation of FAPbI$_3$ perovskite films using the adduct approach where X indicates Lewis bases. (b) Molecular structure of Lewis bases used in this study: dimethyl sulfoxide (DMSO) and *N*-methyl-2-pyrrolidone (NMP). (c, d) Photos and (e, f) scanning electron microscopic (SEM) images of resulting FAPbI$_3$ perovskite films formed using (c, e) DMSO and (d, f) NMP.

formation of PVSK layers based on an adduct approach. The *N,N*-dimethylformamide (DMF) is used as a base solvent to dissolve the adduct complexes because it forms relatively weak interaction with the PVSK precursors owing to its lower basicity.[22] The DMF is removed by washing the film with diethyl ether during spin-coating, which results in the formation of a FAI·PbI$_2$·X adduct film (X is a Lewis base). DMSO and NMP with oxygen bearing lone pair electrons (Figure 1b) were incorporated as Lewis bases in this study. Resulting photos of the films are compared in Figure 1c and d. As can be seen in Figure 1c and d, the FAPbI$_3$ film formed using DMSO (hereafter denoted as FA-DMSO) is inhomogeneous and opaque, likely due to its rough surface. On the contrary, the FAPbI$_3$ film formed with NMP (hereafter denoted as FA-NMP) is highly uniform and semitransparent, which indicates the surface of the film is flat and homogeneous. Absorption spectra of the films are compared in Figure S1, in which the FA-DMSO film shows stronger

absorption over the whole wavelength region. The extended absorption tail of the FA-DMSO film over the band edge region implies the higher absorption is due to the light scattering effect caused by the rough surface of the film.[23] Parts e and f of Figure 1 show surface scanning electron microscopic (SEM) images of the films. The morphology of the FA-DMSO film shows the regional difference, where some part of the film is amorphous-like and contains pinholes and cracks while the other part of the film is relatively uniform but still rough. In the case of the FA-NMP film, the surface of the film is flat, uniform, and pinhole-free, while constitutive grain sizes seem to be relatively small compared to those of the film using DMSO. The smaller grain size of the film with NMP is also correlated with X-ray diffraction spectra in Figure S2. While both films show a cubic FAPbI$_3$ phase with smaller peaks originating from a hexagonal non-PVSK phase (δ) and PbI$_2$ (*), the FA-DMSO film shows a higher intensity of the overall signal and narrower full width at half-maximum (fwhm) than the FA-NMP film.

Characterization of Molecular Interactions. The difference in the morphology of the FAPbI$_3$ film probably originates from the different natures of the intermediate phases resulting from coordinative bonding, as it affects nucleation and growth of the film. The adduct bonding nature was investigated using Fourier transform infrared (FTIR) spectroscopy and density functional theory (DFT) calculation in Figure 2. The FTIR spectra of the DMSO, NMP, and corresponding adducts (see the Methods section in the Supporting Information for details about synthesis) are demonstrated in Figure 2a and f. Figure 2a shows FTIR spectra obtained from DMSO, PbI$_2$·DMSO, and FAI·PbI$_2$·DMSO (full spectra can be found in Figure S3a). The stretching vibration peak of S=O appears around 1050 cm^{-1} for bare DMSO, which is shifted to 1020 cm^{-1} upon formation of the PbI$_2$·DMSO adduct. The decreased stretching vibration frequency of S=O is due to the weakened strength of the S=O bond as a consequence of the dative bond formed by sharing lone pair electrons in oxygen with PbI$_2$.[23] However, the vibration frequency is hardly changed upon addition of FAI, which is consistent with previous reports,[13] indicating coordinative interactions between DMSO and FAI are relatively weak. The spin-coated DMSO adduct solution tends to form an opaque film or to rapidly convert into an opaque film (Figure 2b), indicating the FAI·PbI$_2$·DMSO adduct phase is unstable, which is probably due to the weak interactions between DMSO and FAI. FTIR spectra obtained from NMP, PbI$_2$·NMP, and FAI·PbI$_2$·NMP are shown in Figure 2f (full spectra can be found in Figure S3b). The C=O stretching vibration peak of bare NMP appears at 1685 cm^{-1}, which is shifted to 1654 cm^{-1} in the PbI$_2$·NMP adduct. The peak is further shifted to 1640 cm^{-1} after formation of the FAI·PbI$_2$·NMP adduct, which indicates NMP forms a coordinative bond with both PbI$_2$ and FAI. Contrary to the DMSO adduct solution, the as-spin-coated NMP adduct solution forms a transparent and stable adduct film (Figure 2f). On the basis of this observation, we speculate that NMP forms a relatively stronger and more stable coordinative bond with FAI than DMSO. Such a speculation is also confirmed by investigating the change of the C=N stretch vibration peak of FAI (Figure S4). The C=N stretch vibration peak of bare FAI is observed at 1705 cm^{-1}. The peak position is hardly changed in the FAI·PbI$_2$·DMSO adduct, whereas it is slightly shifted to 1712 cm^{-1} in the FAI·PbI$_2$·NMP adduct, indicating NMP is interacting with FAI.[24] Furthermore, 100 mM FAI solution in NMP shows a light brown color while the other FAI solutions in DMF and DMSO are transparent (Figure S5). The distinctive
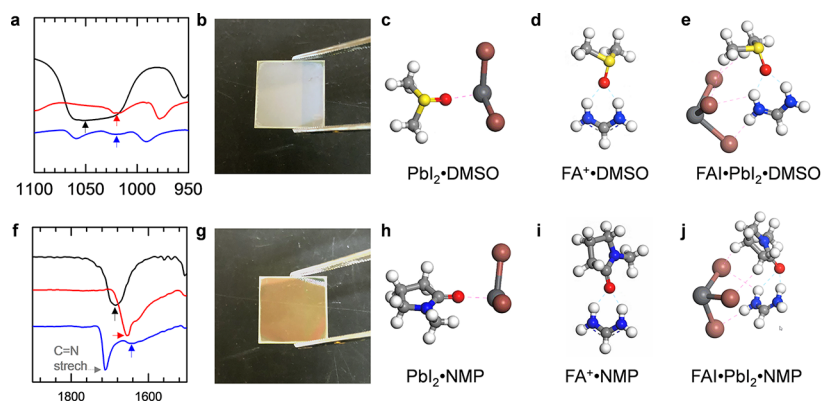
Figure 2. Molecular interaction between perovskite precursors and Lewis bases. Fourier transform infrared spectra for fingerprint regions for (a) S=O and (f) C=O stretching measured from (a) DMSO (solution, black), DMSO + PbI$_2$ (powder, red), and DMSO+PbI$_2$+FAI (powder, blue) and (f) NMP (solution, black), NMP + PbI$_2$ (powder, red), and NMP + PbI$_2$ + FAI (powder, blue). Photos of as-deposited (b) FAI·PbI$_2$·DMSO and (g) FAI·PbI$_2$·NMP adduct films. (c−e, h−j) Molecular structures resulting from DFT calculations: (c) PbI$_2$·DMSO, (d) FA$^+$·DMSO, (e) FAI·PbI$_2$·DMSO, (h) PbI$_2$·NMP, (i) FA$^+$·NMP, and (j) FAI·PbI$_2$·NMP.

color of FAI dissolved in NMP is probably due to the formation of a charge transfer complex. For investigation of the molecular interaction between the Lewis bases and FAI in precursor solution, we compared the FTIR spectra of the FAI solution in the Lewis bases. We used the attenuated total reflection (ATR) mode to enhance the accuracy of the measurement with liquid samples. The molar ratio between the FAI and Lewis bases was varied to see the correlation between the interaction and characteristic peak positions. As seen in Figure S6a and b, DMSO and NMP show the shifts of characteristic stretching vibration peaks (S=O for DMSO and C=O for NMP) toward lower wavenumbers upon addition of FAI, which is indicative of the interaction with FAI. The stretch vibration peak of S=O in DMSO is shifted from 1042 (bare DMSO) to 1014, 1012, and 1010 cm^{-1} when the molar ratio of DMSO to FAI is 4:1, 3:1, and 2:1, respectively. Similarly, the stretch vibration peak of C=O in NMP is shifted from 1673 (bare NMP) to 1656, 1651, and 1650 cm^{-1} when the ratio of NMP to FAI is 4:1, 3:1, and 2:1, respectively. However, it is difficult to quantify the strength of the interaction because two bonds associated with DMSO and NMP are different. Alternatively, we compared the C=N stretching vibration peak of FAI with two different Lewis bases. The formation of a hydrogen bond between the amine functional groups of FAI and Lewis base is likely to strengthen the C=N bond of FAI, and therefore, a blue-shift of the C=N stretching vibration peak is expected. As seen in Figure S6c and d, the C=N stretch vibration peak of FAI is shifted toward a higher wavenumber when FAI interacts with DMSO and NMP. The stretch vibration peak of C=N in FAI is shifted from 1693 (bare FAI) to 1710, 1714, and 1717 cm^{-1} when the ratio of DMSO to FAI is 4:1, 3:1, and 2:1, respectively. In the case of NMP, the vibration peak of C=N is shifted from 1693 to 1712, 1716, and 1719 cm^{-1} when the ratio of NMP to FAI is 4:1, 3:1, and 2:1, respectively. The more pronounced shift of the peak with NMP implies stronger interaction of FAI with NMP than that of DMSO, which correlates to the FAI·PbI$_2$·NMP adduct being more stable than FAI·PbI$_2$·DMSO. The unstable intermediate phase with DMSO is expected to induce heterogeneous nucleation, as it contains a solid phase of precursors or PVSK. Poor coverage and inhomogeneous morphology of the FA-DMSO film is probably due to the heterogeneous nucleation. Thermogravimetric analysis (TGA) of the adduct powders is carried out in Figure S7. Weight loss at a relatively low

temperature (<250 °C) can be attributed to evaporation of DMSO or NMP. The FAI·PbI$_2$·DMSO adduct powder shows two distinct weight losses at around 70 and 190 °C, whereas FAI·PbI$_2$·NMP adduct powder shows single weight loss at around 70 °C. We speculate that the two distinct weight losses observed from the FAI·PbI$_2$·DMSO adduct are probably due to the presence of secondary phases, i.e., pure DMSO or PbI$_2$·DMSO$_n$ due to the instability of the FAI·PbI$_2$·DMSO adduct.

We simulated molecular interactions to calculate interaction energies for the DMSO and NMP adducts. The stabilized molecular structures are demonstrated in Figure 2c−e and h−j, while the calculated interaction energies are summarized in Table S1. As expected, PbI$_2$ interacts with the oxygen in DMSO and NMP (Figure 2c and h). The interaction energies of the bonding were calculated to be −0.731 eV for PbI$_2$·DMSO and −0.675 eV for PbI$_2$·NMP. The stronger interaction of PbI$_2$ with DMSO is probably due to the higher donor number of DMSO (29.8) than NMP (27.3).[22] The FA cation is found to interact with DMSO and NMP through hydrogen bonding as reported previously (Figure 2d and i).[25,26] The interaction energy between the FA cation and DMSO is calculated to be −1.253 eV, which is lower than that between the FA cation and NMP (−1.407 eV). This is correlated with experimental observation. The molecular geometries of FAI·PbI$_2$·DMSO and FAI·PbI$_2$·NMP adducts are demonstrated in Figure 2e and j. Considering that the solubility of PbI$_2$ in N,N-dimethylformamide (DMF) is enhanced in the presence of MAI or FAI, it is likely that solvation of FAI or MAI provides the iodide (I$^-$) to react with PbI$_2$ to form iodoplumbate anions (PbI$_3^-$).[27] The presence of iodoplumbate anions in PVSK precursor solution has been proven by characteristic absorption peaks observed from the absorption spectrum of the PVSK solution.[28] As a result, crystallization of iodoplumbate salts such as (MA$^+$)$_2$[(PbI$_3^-$)$_2$·DMF$_2$] has been reported from the solution, in which the PbI$_3^-$ network is stabilized by the hydrogen-bonded network of MA$^+$·DMF.[25] Therefore, we adopted the molecular structure of (FA$^+$)·(PbI$_3^-$)·(DMSO or NMP) in order to calculate the interaction energies. The higher interaction energy of FAI·PbI$_2$·NMP (−2.413 eV) than that of FAI·PbI$_2$·DMSO (−2.138 eV) is well correlated with more stable FAI·PbI$_2$·NMP than FAI·PbI$_2$·DMSO adducts. The calculated molecular geometries in Figure 2e and j show the highest interaction energies in which the oxygen with lone pair electrons in DMSO and NMP preferentially interacts with FA cation in FAI·PbI$_2$·

DMSO and FAI·PbI$_2$·NMP adducts. This is probably due to the relatively stronger interaction energies of NMP and DMSO with FA cation. We also considered the geometry with interaction of the oxygen with both FA cations and Pb atoms, as seen in Figure S8. Regardless of the lower overall interaction energies, the FAI·PbI$_2$·NMP still shows a stronger interaction energy (−0.999 eV) than that of FAI·PbI$_2$·DMSO (−0.874 eV).

Considerations for Selecting the Lewis Bases. We paid attention to the molecular structure of DMSO and NMP for unraveling the origin of the different molecular interactions. We adopted different Lewis bases for confirming the criteria (Figure 3, the properties of the solvents are summarized in Table S2[29]). We derived the following criteria:
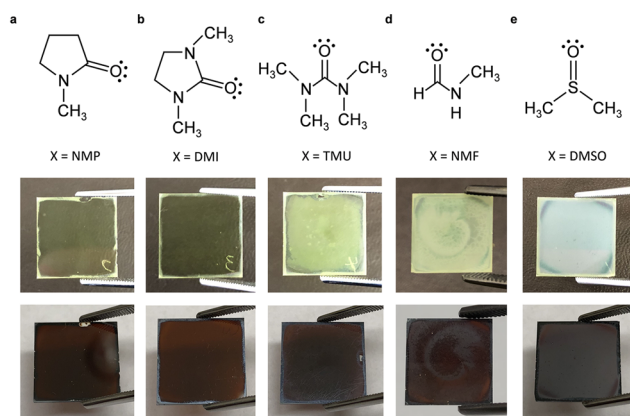

Figure 3. Film formation with different Lewis bases. Molecular structures of the Lewis bases (upper panel) and corresponding adduct (middle panel) and perovskite films (lower panel). The perovskite solutions were prepared by mixing 1 mmol of FAI, PbI$_2$, and corresponding Lewis base in 760 mg of DMF.

1. High Hydrogen Bond Accepting Ability and Low Hydrogen Bonding Donor Ability. Higher hydrogen bond accepting (HBA) ability of the Lewis base is desired because FA cation forms a hydrogen bond with the Lewis base. However, if the Lewis base also has a sufficiently Lewis acidic functional group (such as a primary or secondary amide possessing a N−H bond) that can serve as a hydrogen bond donor, the Lewis base will tend to form a hydrogen bond with another molecule of the Lewis base and dimerize (for example, urea is well-known to self-associate due to its Lewis basic oxygen hydrogen bonding with amide N−H bonds[30]). Such a Lewis base will result in a competition between the acidic functional group and FA cation molecules and weakening of the interaction between the Lewis base and FA cation molecules. Therefore, lower Lewis acidity is favorable. The NMP has a higher HBA ability (β = 77) and a lower Lewis acidity (acceptor number, AN = 13.3) than that of DMSO (β = 76, AN = 19.3), which results in more effective hydrogen bonding of NMP with FA cation than that of DMSO. We tried *N*-methylformamide (NMF) that has a high HBA ability (β = 80) but also a very high acceptor number (AN = 32.1), which is comparable to even some of the alcohols (isopropanol, AN = 33.5, *tert*-butanol, AN = 27.1). NMF could not form a stable adduct film (Figure 3d), most likely due to its high AN, resulting in the competition of NMF with FA cation molecules.

2. Sterically Accessible Electron Donating Atom. In both NMP and DMSO, the oxygen with lone pair electrons acts as an electron donor to form hydrogen bonds. We hypothesized that

the oxygen in NMP is more sterically accessible because it protrudes out from the cyclic scaffold with only one methyl group in the α position of the carbonyl, whereas the oxygen in DMSO is sterically hindered by two adjacent methyl groups that are free to rotate due to the linear (acyclic) structure of DMSO. To test this hypothesis about cyclic structure, we compared 1,3-dimethyl-2-imidazolidinone (DMI) and tetramethylurea (TMU), which are almost identical molecules except the two methyl groups in TMU are linked by a covalent bond in DMI to form a 5-membered ring. TMU has high β = 80 and low AN = 9.2, so it satisfies criteria 1, and DMI is expected to have very similar β and AN, since it possesses identical functional groups and number of carbons. The only difference is that DMI has a cyclic structure, whereas TMU has a linear structure. We observed that DMI is able to form a stable and uniform adduct film, whereas TMU cannot form the stable adduct film (Figure 3b and c). This result suggests that the steric environment around the Lewis basic oxygen greatly affects film forming ability; in other words, the oxygen atom of cyclic DMI is more sterically accessible than that of linear TMU and results in better film quality for DMI. When the steric hindrance around the oxygen atom is further reduced by replacing DMI with NMP, which has only one alpha methyl group compared to two alpha methyl groups in DMI, we observed more reproducible adduct films when using NMP than DMI.

3. Matching the Hardness and Softness of the Lewis Acid and Base. DMSO is able to form a uniform and stable adduct film with MAI and PbI$_2$, whereas NMP cannot form the stable adduct film with MAI and PbI$_2$ (Figure S9). This observation suggests that there might be another factor responsible for the selectivity (the FA cation preferentially interacts with NMP over DMSO, whereas the MA cation preferentially interacts with DMSO over NMP). This should arise from the different molecular interaction of the Lewis bases and FA or MA cation. Indeed, the DFT calculations (Table S3 and Figure S9) show that DMSO has a stronger interaction energy (−1.391 eV) with MA cation than with NMP (−1.210 eV), and thus, the interaction energy of MAI·PbI$_2$·DMSO (−1.619 eV) is stronger than that of MAI·PbI$_2$·NMP (−1.541 eV). This trend is completely opposite for the FA cation, for which the interaction energy is stronger with NMP (−1.407 eV) than with DMSO (−1.253 eV) (Table S1). We attribute the preference of DMSO to interact with MA cation and NMP to interact with FA cation to the hard and soft acids and bases (HSAB) concept. The charges in FA$^+$ are relatively delocalized due to the resonance contribution from the C−N bonds, resulting in the lower dipole moment (0.21 D) compared to MA cation (2.29 D).[31] According to the HSAB concept, FA cation is a softer Lewis acid than MA cation, so it preferentially interacts with a soft base and vice versa for MA cation. NMP has a higher polarizability (10.66 Å^3) than DMSO (8.03 Å^3)[32] and therefore is a softer base compared to DMSO. Therefore, FA cation preferentially interacts with NMP over DMSO, whereas MA cation preferentially interacts with DMSO over NMP.

Correlation between Morphology and Device Performance. PVSK solar cells were fabricated using the FA-DMSO and FA-NMP films, in which the devices incorporate a planar heterojunction structure (ITO/compact-SnO$_2$/FAPbI$_3$/spiro-MeOTAD/Ag). Cross-sectional SEM images of the devices incorporating FA-DMSO and FA-NMP films are demonstrated in Figure 4. Rough top surfaces of the FA-DMSO film can be seen from Figure 4a and c. Also, the film shows poor contact with SnO$_2$ coated ITO substrates, in which a
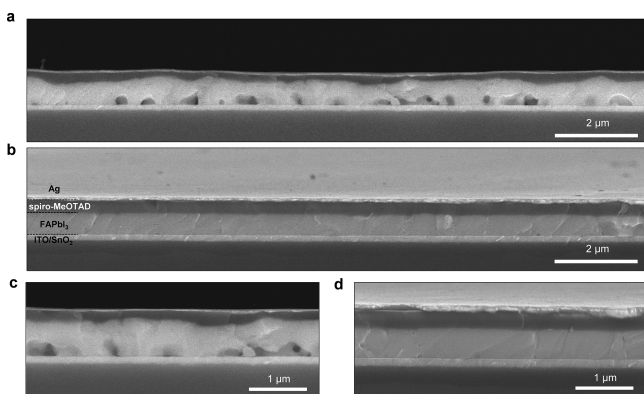
Figure 4. Cross-sectional morphology of the devices. Cross-sectional scanning electron microscopic images of planar heterojunction FAPbI$_3$ perovskite solar cells using (a, c) DMSO and (b, d) NMP. The structure of the devices was ITO/compact SnO$_2$/FAPbI$_3$/spiro-MeOTAD/Ag. (a, b) Lower magnification and (c, d) higher magnification images.

lot of microscaled voids are observed. On the contrary, FA-NMP film is highly uniform and shows better contact with both SnO$_2$ and spiro-MeOTAD layers. Uniform and controlled crystallization of the PVSK layer from stable intermediate adduct phases with NMP may facilitate better contact with the underlying SnO$_2$ layer. One can relate the poor contact of FA-DMSO film to poor wettability of the PVSK solution. The contact angles of the PVSK solutions on SnO$_2$ coated ITO glass were measured in Figure S10. The contact angle of the PVSK solution based on DMSO is measured to be 22.2° (Figure S10a), while that of the solution based on NMP is measured to be 15.0° (Figure S10b), which indicates a better wettability of the solution

based on NMP. The better wettability of the solution based on NMP is probably due to the lower surface tension of NMP (40.79 mN/m) than that of DMSO (44.0 mN/m). However, we performed UV-ozone treatment on the substrate before spin-coating of the PVSK solutions and in such a case both of the solutions based on DMSO and NMP show almost perfect wetting on the substrate (Figure S10c and d). Therefore, the difference in morphology seems to predominantly result from the difference in molecular interactions. Actually, it was reported that the nonwetting surface of the substrate can induce the formation of PVSK film with larger grain size due to enhanced grain boundary mobility during crystal growth,[33] which is in agreement with the larger grain size of the PVSK film formed from the solution based on DMSO.

Photovoltaic parameters of the devices are compared in Figure 5 and Table 1. While the average short-circuit current densities (J_{SC}) of devices with FA-NMP film (23.19 ± 0.32 mA/cm^2) are comparable with those of devices with FA-DMSO films (23.21 ± 0.41 mA/cm^2), open-circuit voltages (V_{OC}) and fill factors (FF) are improved by 3.7% (from 0.995 ± 0.045 to 1.032 ± 0.019 V) and 15.2% (from 0.604 ± 0.028 to 0.696 ± 0.014) with FA-NMP film. Thus, the average power conversion efficiency (PCE) of the devices is significantly improved by 19.1% from 13.97 ± 1.32 to 16.64 ± 0.59%. Also, superior reproducibility of the devices incorporating the FA-NMP films can be attributed to the better uniformity of the films. The FA-NMP film contains fewer pinholes than the FA-DMSO, so a smaller leakage current and higher shunt resistance will enhance the V_{OC} and FF. Furthermore, better contact with the underlying SnO$_2$ layer will facilitate charge extraction and reduce the series resistance. Such speculation is supported by dark $J-V$ curve measurement (inset of Figure 5e and f). Series and shunt resistance (R_s and R_{sh},
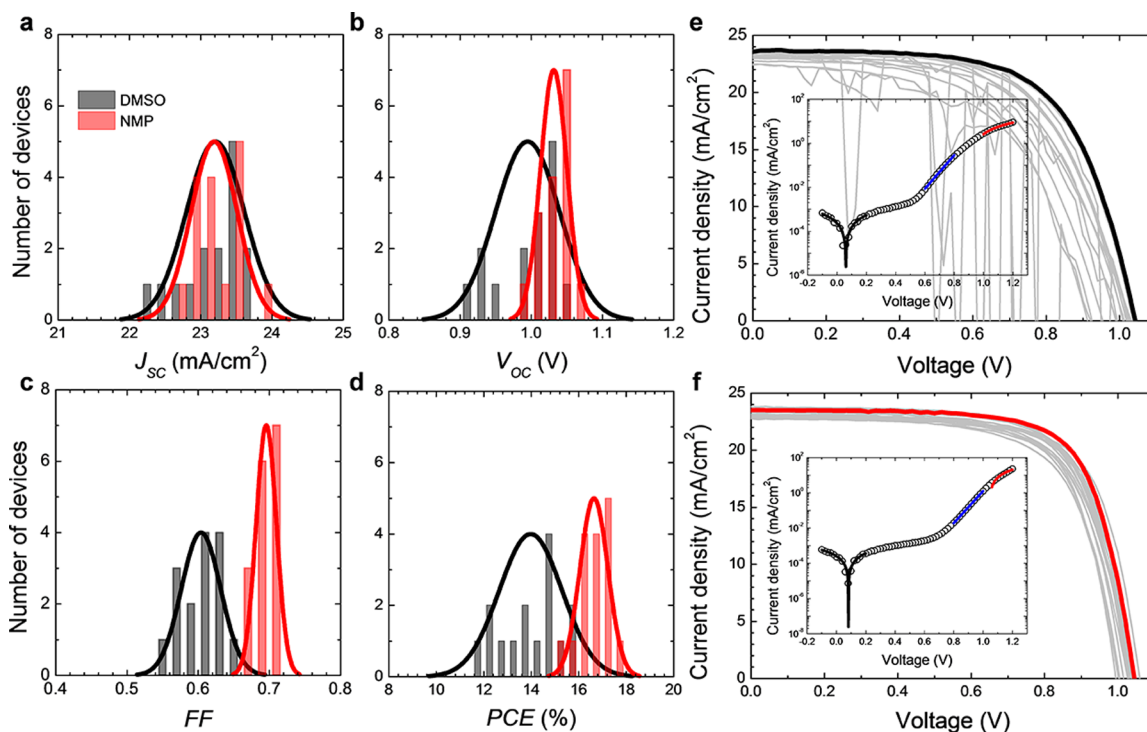

Figure 5. Effect of Lewis bases on photovoltaic performance. Photovoltaic parameters of the perovskite solar cell based FAPbI$_3$ formed using DMSO and NMP. (a) Short-circuit current density (J_{SC}), (b) open-circuit voltage (V_{OC}), (c) fill factor (FF), and (d) power conversion efficiency (PCE). Corresponding current density–voltage ($J-V$) curves of the devices using (e) DMSO and (f) NMP. The insets of parts e and f show dark $J-V$ curves for the devices. Empty circles are measured data, and solid lines are a linear fit of the data.

Table 1. Photovoltaic Parameters of the FAPbI$_3$ Perovskite Solar Cells Formed Using DMSO and NMP[a]

device ID	J_{SC} (mA/cm^2)	V_{OC} (V)	FF	PCE (%)
DMSO	23.21 ± 0.41	0.995 ± 0.045	0.604 ± 0.028	13.97 ± 1.32
NMP	23.19 ± 0.32	1.032 ± 0.019	0.696 ± 0.014	16.64 ± 0.59
	R_s (Ω cm^2)	R_{sh} (Ω cm^2)	J_0 (mA/cm^2)	n
DMSO	33.1	261780.1	2.27×10^{-7}	1.46
NMP	7.3	318471.3	9.74×10^{-10}	1.22

[a]The average short-circuit current density (J_{SC}), open-circuit voltage (V_{OC}), fill factor (FF), and power conversion efficiency (PCE) are listed. The series resistance (R_s), shunt resistance (R_{sh}), saturation current (J_0), and ideality factor (n) calculated from current density−voltage curves measured under dark are also provided.
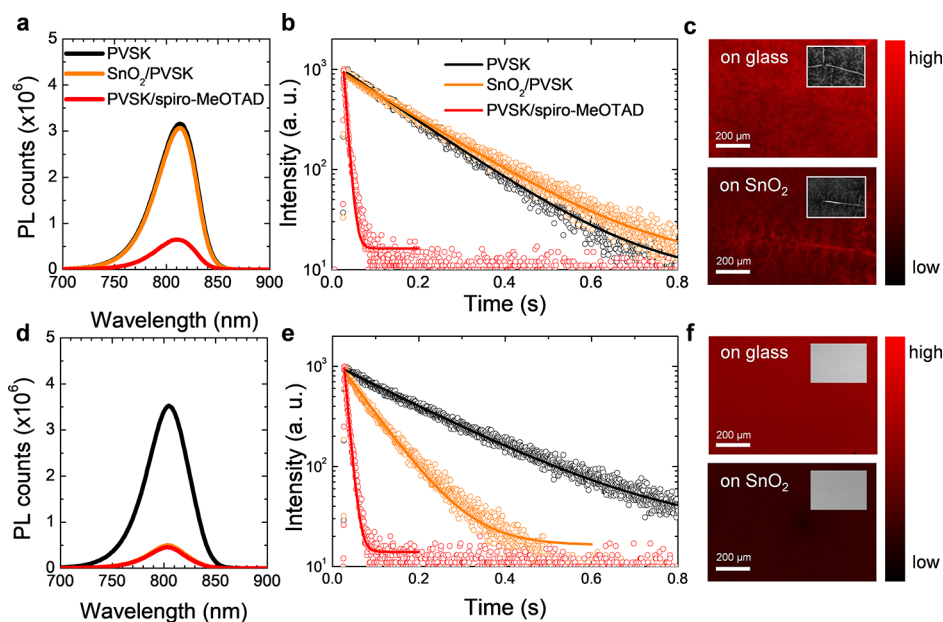

Figure 6. Effect of Lewis bases on photoluminescence properties. (a, d) Steady-state and (b, e) time-resolved photoluminescence (PL) spectra of FAPbI$_3$ perovskite films in contact with a bare glass substrate, SnO$_2$ layer, and spiro-MeOTAD layer. The FAPbI$_3$ films were formed using (a, b) DMSO and (d, e) NMP. PL mapping of the FAPbI$_3$ films formed using (c) DMSO and (f) NMP on a glass substrate and SnO$_2$ coated ITO glass. The insets of parts c and f show corresponding electron images of the films in the same scale.

respectively) were calculated from the inverse of the slope near the short- and open-circuit regions.

Empty circles are measured data, and solid lines are a linear fit of the data. The ideality factor (n) and saturation current (J_0) were obtained by fitting the $J-V$ curve to the following diode equation[34]

$$\ln(J_D) = \ln(J_0) + \left(\frac{1}{n}\right)\frac{q}{k_B T}V_b$$

where J_D is the current density, q is an elemental charge, k_B is the Boltzmann constant, and T is the temperature. The fitted parameters are listed in Table 1. The device incorporating FA-NMP film shows a lower series resistance (7.3 Ω cm^2) and higher shunt resistance (318471.3 Ω cm^2) than those of the device incorporating FA-DMSO (R_s = 33.1 Ω, R_{sh} = 261780.1 Ω), which is the origin of the higher FF of the FA-NMP devices. Also, the lower J_0 of the device with the FA-NMP film is correlated with its higher V_{OC} than that of the FA-DMSO device.[35]

Photoluminescence Properties and Best Performance. To correlate the morphology of the film with the photovoltaic performance and electrical properties of the devices, photogenerated charge behavior was investigated using photoluminescence (PL) measurements in Figure 6. Fitted parameters for time-resolved PL profiles are summarized in Table S4, in

which τ_{bare}, τ_{ETL}, and τ_{HTL} indicate calculated PL lifetimes of the PVSK films in contact with a bare glass substrate, SnO$_2$ layer, and spiro-MeOTAD layer, respectively. The steady-state PL intensity of the FA-NMP film on a glass substrate is slightly higher than that of the FA-DMSO film (Figure 6a and d), which is in agreement with the longer PL lifetime of the FA-NMP film (τ_{bare} = 199.0 ns) than that of FA-DMSO (τ_{bare} = 147.2 ns), shown in Figure 6b and e. The reduced steady-state PL intensity and shortened PL lifetime ($\tau_{HTL} \sim 8$ ns) of the films in contact with spiro-MeOTAD are observed for both films, which indicates photogenerated hole extraction from the PVSK layer to spiro-MeOTAD is efficient. However, the FA-DMSO film in contact with a SnO$_2$ layer shows comparable PL intensity and lifetime (τ_{ETL} = 163.0 ns) with the bare FA-DMSO film, whereas a clear PL quenching with a decreased PL lifetime (τ_{ETL} = 72.4 ns) is observed from FA-NMP in contact with the SnO$_2$ layer. This is correlated with poor contact of the FA-DMSO film with the SnO$_2$ layer (Figure 4), which will hinder efficient electron extraction from the PVSK film to SnO$_2$. Parts c and f of Figure 6 show PL mapping images of the FA-DMSO and FA-NMP film, respectively. Uniformity of the PL intensity on a glass substrate is more superior in the FA-NMP film than FA-DMSO. Upon contacting with SnO$_2$ coated ITO substrate, the PL signal from the FA-DMSO film is partially quenched while that of FA-NMP
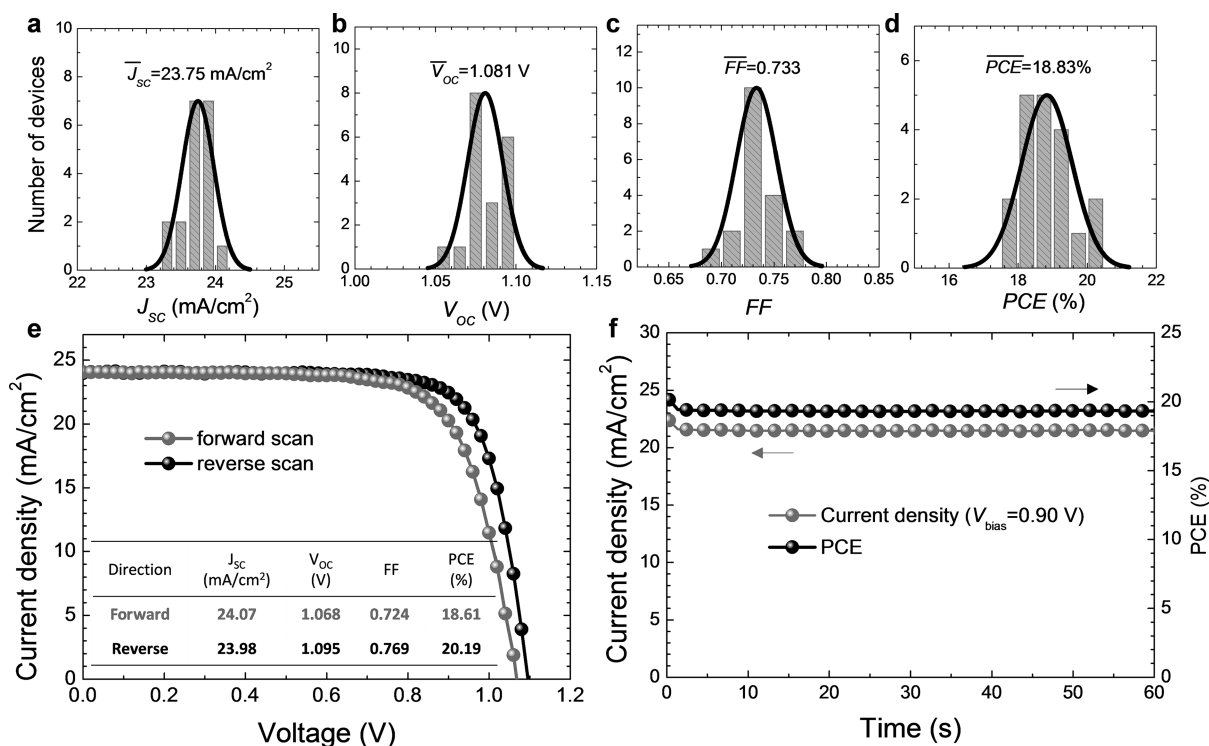
Figure 7. Reproducible and efficient $FA_{0.98}Cs_{0.02}PbI_3$ perovskite solar cells. Distribution of photovoltaic parameters measured from perovskite solar cells based on $FA_{0.98}Cs_{0.02}PbI_3$. (a) Short-circuit current density (J_{SC}), (b) open-circuit voltage (V_{OC}), (c) fill factor (FF), and (d) power conversion efficiency (PCE). (e) Current density−voltage ($J-V$) curves and (f) steady-state efficiency measurement for the best performing $FA_{0.98}Cs_{0.02}PbI_3$ perovskite solar cell. The applied bias voltage for steady-state measurement was 0.90 V.

film is quenched uniformly, which is in accordance with the steady-state and time-resolved PL measurement.

Although the morphology of the $FAPbI_3$ film is improved, the inevitable formation of the secondary phase (hexagonal non-PVSK phase, δ in Figure S2) might degrade the photovoltaic performance. The phase purity can be improved by incorporating a small amount of cesium cation as previously reported.[16,36] We incorporated 2 mol % of cesium (Cs), and the XRD pattern of the film is demonstrated in Figure S11. The XRD pattern of the $FA_{0.98}Cs_{0.02}PbI_3$ film does not contain the non-PVSK phase, and the overall intensity and fwhm of the peaks are enhanced compared to the bare $FAPbI_3$ film using NMP. The distribution of the photovoltaic parameters measured from the PVSK solar cells based on the $FA_{0.98}Cs_{0.02}PbI_3$ is demonstrated in Figure 7a–d. Compared to bare $FAPbI_3$ devices (Figure 5 and Table 1), the improved J_{SC}, V_{OC}, and FF led to an average PCE improved by 13.2% from 16.64 ± 0.59 to 18.83 ± 0.73%, which can be attributed to enhanced phase purity and crystallinity of the PVSK layer. The $J-V$ curves and steady-state PCE of the best performing device are demonstrated in Figure 7e and f. The forward and reverse $J-V$ scans yield a PCE of 18.61% (J_{SC}, 24.07 mA/cm²; V_{OC}, 1.068 V; FF, 0.724) and a PCE of 20.19% (J_{SC}, 23.98 mA/cm²; V_{OC}, 1.095 V; FF, 0.769), respectively. The steady-state PCE of the device was measured to be 19.34% under a constant bias voltage of 0.90 V. The external quantum efficiency (EQE) of the device is demonstrated in Figure S12, where the integrated J_{SC} was calculated to be 22.40 mA/cm². The 7.1% of discrepancy comparing with J_{SC} measured in the $J-V$ curve is probably due to the capacitive current owing to $J-V$ hysteresis.

CONCLUSIONS

In this report, we introduced an efficient method to form a high-quality $FAPbI_3$ film via an adduct approach. Replacement of the typical Lewis base DMSO with NMP enabled the formation of a stable intermediate $FAI \cdot PbI_2 \cdot NMP$ adduct, resulting in an uniform and reproducible $FAPbI_3$ film. Investigation of FT-IR spectra revealed that NMP forms a stronger coordinative bond with FAI than DMSO, which was thought to be the origin of the better stability of the adduct with NMP than DMSO. Such experimental observation was correlated with DFT calculations, in which the interaction energy of NMP with the FA cation was higher than DMSO. From this study, we conclude that the molecular interactions between FA or MA cation and Lewis bases play a crucial role in the stability of the resulting adduct films. Although many factors still exist to be explored for selecting proper Lewis bases for the adduct approach, based on our findings, we propose these criteria for selecting Lewis bases: (1) high hydrogen bond accepting ability and low hydrogen bonding donor ability, (2) sterically accessible electron donating atom, and (3) matching the hardness and softness of Lewis acid and base. As a result of the high film quality, the PVSK solar cell with the highest PCE over 20% (stabilized PCE of 19.34%) and average PCE of 18.83 ± 0.73% was demonstrated. We believe this report will provide a methodological base to further enhance the performance and stability of PVSK solar cells using formamidinium based PVSK.

ASSOCIATED CONTENT

ⓈSupporting Information

The Supporting Information is available free of charge on the ACS Publications website at DOI: 10.1021/jacs.8b01037.

Experimental details, Figures S1–S12, and Tables S1–S4 (PDF)

■ AUTHOR INFORMATION

Corresponding Author
*yangy@ucla.edu

ORCID ⓘ
Bruce Dunn: 0000-0001-5669-4740
Heather D. Maynard: 0000-0003-3692-6289
Yang Yang: 0000-0001-8833-7641

Author Contributions
[1]J.-W.L., Z.D.: These authors contributed equally to this work.

Notes
The authors declare no competing financial interest.

■ REFERENCES

(1) Kojima, A.; Teshima, K.; Shirai, Y.; Miyasaka, T. *J. Am. Chem. Soc.* **2009**, *131*, 6050.

(2) Im, J.-H.; Lee, C.-R.; Lee, J.-W.; Park, S.-W.; Park, N.-G. *Nanoscale* **2011**, *3*, 4088.

(3) Kim, H.-S.; Lee, C.-R.; Im, J.-H.; Lee, K.-B.; Moehl, T.; Marchioro, A.; Moon, S.-J.; Humphry-Baker, R.; Yum, J.-H.; Moser, J. E. *Sci. Rep.* **2012**, *2*, 591.

(4) Lee, M. M.; Teuscher, J.; Miyasaka, T.; Murakami, T. N.; Snaith, H. J. *Science* **2012**, *338*, 643.

(5) National renewable energy laboratory, Best research-cell efficiency chart, https://www.nrel.gov/pv/assets/images/efficiency-chart.png.

(6) Lee, J. W.; Seol, D. J.; Cho, A. N.; Park, N. G. *Adv. Mater.* **2014**, *26*, 4991.

(7) Xing, G.; Mathews, N.; Sun, S.; Lim, S. S.; Lam, Y. M.; Grätzel, M.; Mhaisalkar, S.; Sum, T. C. *Science* **2013**, *342*, 344.

(8) Stranks, S. D.; Eperon, G. E.; Grancini, G.; Menelaou, C.; Alcocer, M. J.; Leijtens, T.; Herz, L. M.; Petrozza, A.; Snaith, H. J. *Science* **2013**, *342*, 341.

(9) Yin, W.-J.; Shi, T.; Yan, Y. *Appl. Phys. Lett.* **2014**, *104*, 063903.

(10) Nagabhushana, G.; Shivaramaiah, R.; Navrotsky, A. *Proc. Natl. Acad. Sci. U. S. A.* **2016**, *113*, 7717.

(11) Lee, J.-W.; Bae, S.-H.; Hsieh, Y.-T.; De Marco, N.; Wang, M.; Sun, P.; Yang, Y. *Chem.* **2017**, *3*, 290.

(12) Ahn, N.; Son, D.-Y.; Jang, I.-H.; Kang, S. M.; Choi, M.; Park, N.-G. *J. Am. Chem. Soc.* **2015**, *137*, 8696.

(13) Lee, J.-W.; Kim, H.-S.; Park, N.-G. *Acc. Chem. Res.* **2016**, *49*, 311.

(14) Park, N.-G. *Inorg. Chem.* **2017**, *56*, 3.

(15) Son, D.-Y.; Lee, J.-W.; Choi, Y. J.; Jang, I.-H.; Lee, S.; Yoo, P. J.; Shin, H.; Ahn, N.; Choi, M.; Kim, D. *Nat. Energy* **2016**, *1*, 16081.

(16) Lee, J. W.; Kim, D. H.; Kim, H. S.; Seo, S. W.; Cho, S. M.; Park, N. G. *Adv. Energy Mater.* **2015**, *5*, 1501310.

(17) Jeon, N. J.; Noh, J. H.; Yang, W. S.; Kim, Y. C.; Ryu, S.; Seo, J.; Seok, S. I. *Nature* **2015**, *517*, 476.

(18) Son, D.-Y.; Kim, S.-G.; Seo, J.-Y.; Lee, S.-H.; Shin, H.; Lee, D.; Park, N.-G. *J. Am. Chem. Soc.* **2018**, *140*, 1358.

(19) Slotcavage, D. J.; Karunadasa, H. I.; McGehee, M. D. *ACS Energy Lett.* **2016**, *1*, 1199.

(20) Bischak, C. G.; Hetherington, C. L.; Wu, H.; Aloni, S.; Ogletree, D. F.; Limmer, D. T.; Ginsberg, N. S. *Nano Lett.* **2017**, *17*, 1028.

(21) Eperon, G. E.; Stranks, S. D.; Menelaou, C.; Johnston, M. B.; Herz, L. M.; Snaith, H. J. *Energy Environ. Sci.* **2014**, *7*, 982.

(22) Cataldo, F. *Eur. Chem. Bull.* **2015**, *4*, 92.

(23) Seol, D. J.; Lee, J. W.; Park, N. G. *ChemSusChem* **2015**, *8*, 2414.

(24) Purcell, K. F.; Drago, R. S. *J. Am. Chem. Soc.* **1966**, *88*, 919.

(25) Guo, Y.; Shoyama, K.; Sato, W.; Matsuo, Y.; Inoue, K.; Harano, K.; Liu, C.; Tanaka, H.; Nakamura, E. *J. Am. Chem. Soc.* **2015**, *137*, 15907.

(26) Petrov, A. A.; Sokolova, I. P.; Belich, N. A.; Peters, G. S.; Dorovatovskii, P. V.; Zubavichus, Y. V.; Khrustalev, V. N.; Petrov, A. V.; Grätzel, M.; Goodilin, E. A. *J. Phys. Chem. C* **2017**, *121*, 20739.

(27) Krautscheid, H.; Vielsack, F. *J. Chem. Soc., Dalton Trans.* **1999**, 2731.

(28) Rahimnejad, S.; Kovalenko, A.; Forés, S. M.; Aranda, C.; Guerrero, A. *ChemPhysChem* **2016**, *17*, 2795.

(29) Marcus, Y. *Chem. Soc. Rev.* **1993**, *22*, 409.

(30) Roberts, J. M.; Fini, B. M.; Sarjeant, A. A.; Farha, O. K.; Hupp, J. T.; Scheidt, K. A. *J. Am. Chem. Soc.* **2012**, *134*, 3334.

(31) Frost, J. M.; Butler, K. T.; Brivio, F.; Hendon, C. H.; Van Schilfgaarde, M.; Walsh, A. *Nano Lett.* **2014**, *14*, 2584.

(32) Bosque, R.; Sales, J. *Journal of chemical information and computer sciences* **2002**, *42*, 1154.

(33) Bi, C.; Wang, Q.; Shao, Y.; Yuan, Y.; Xiao, Z.; Huang, J. *Nat. Commun.* **2015**, *6*, 7747.

(34) Kang, H.-W.; Lee, J.-W.; Son, D.-Y.; Park, N.-G. *RSC Adv.* **2015**, *5*, 47334.

(35) Cuevas, A. *Energy Procedia* **2014**, *55*, 53.

(36) Saliba, M.; Matsui, T.; Seo, J.-Y.; Domanski, K.; Correa-Baena, J.-P.; Nazeeruddin, M. K.; Zakeeruddin, S. M.; Tress, W.; Abate, A.; Hagfeldt, A. *Energy Environ. Sci.* **2016**, *9*, 1989.